

X-ray observation of the super-luminal quasar 4C +73.18 (1928+738) by ASCA

W. Yuan^{1,2,3,4}, W. Brinkmann¹, M. Gliozzi¹, Y. Zhao³, and M. Matsuoka⁴

¹ Max-Planck-Institut für extraterrestrische Physik, Giessenbachstrasse, D-85740 Garching, Germany

² Beijing Astrophysics Center (BAC), No.1 Yifu Building 5501, Peking University, Beijing 100871 China

³ Beijing Astronomical Observatory, National Astronomical Observatories, Chinese Academy of Sciences, Beijing 100012, China

⁴ National Space Development Agency of Japan (NASDA), Tsukuba Space Center, 2-1-1 Sengen, Tsukuba, Ibaraki 305 Japan

Received Sep. 1, 1999; accepted Feb. 24, 2000

Abstract. The results of an X-ray observation of the nearby core-dominated, super-luminal quasar 4C +73.18 (1928+738) with ASCA are reported. Variations of the 1–10 keV flux on time-scales of the order of 10 hours were found while the 0.5–1 keV flux remained almost unchanged. The measured flux at 1 keV had increased by $\sim 50\%$ compared with previous observations 18 years ago. The quasar shows a curved spectrum in the 0.8–10 keV band, which can be modeled as a power law plus a soft component. Both, the spectrum and the uncorrelated flux variations indicate the presence of a soft X-ray excess over the extrapolation of the hard band power law, which might be the high-energy extension of the intense UV bump emission found in this quasar. The hard X-ray emission is dominated by the flat power law (photon index 1.1–1.5). The results are consistent with models in which the hard X-rays are emitted from the relativistic jet. An iron line emission as reported in a previous Ginga observation (Lawson & Turner 1997) was not detected. We suggest that the line detected by Ginga might be not associated with the quasar but, most likely, with a distant cluster of galaxies. There are indications for a weak emission line-like feature around 1.25 keV (1.63 keV in the quasar frame) in both, the SIS and GIS spectra. The energy is surprisingly close to that of an unexplained line found in the flat-spectrum quasar PKS 0637-752 by Yaqoob et al. (1998). No evidence for the proposed binary black holes (Roos et al. 1993) is found in the current X-ray data.

Key words: Galaxies: quasars: individual: 4C +73.18 (1928+738)– X-rays: galaxies

1. Introduction

4C +73.18 (1928+738) is an extremely core-dominated, super-luminal quasar at a redshift of 0.302. It is a flat-spectrum radio source in the S5 survey (Kühr et al. 1981), which has been well studied with VLBI and shows unusual jet properties. On arc-second (kpc) scales, the source exhibits two-sided curved jets, lobes, and a dominant core (Johnston et al. 1987, Hummel et al. 1992, Murphy et al. 1993). On pc scales, VLBI observations of the core reveal an one-sided jet, which exhibits apparent super-luminal motion with $v_{\text{app}}/c \sim 4 - 7$ (Eckart et al. 1985, Witzel et al. 1988). The jet is estimated to be aligned within $7^\circ - 12^\circ$ to the line-of-sight (e.g. Ghisellini et al. 1993, Jiang et al. 1998). No γ -ray emission was detected by EGRET (Fichtel et al. 1994). To explain the mis-alignment between the VLBI jet and the kpc-scale jet, Hummel et al. (1992) suggested that the observed VLBI jet might be only one of the Doppler-boosted filaments. Interestingly, the most recent results from the space VLBI (VSOP) monitoring of 4C +73.18 reveal substantial jet bending at a distance of 6.3 pc from the core, and dramatic temporal variations of the bend angle over a few months (Murphy et al. 1999).

It is intriguing that the sub-milliarcsec jet exhibits ballistic motion along a sinusoidal curve with a period of about 3 years (Hummel et al. 1992). The wiggles over such short period were modeled by Roos et al. (1993) as the orbital motion of a binary black hole system, which has a mass of the order of $10^8 M_\odot$, a mass ratio > 0.1 , and a separation of $\sim 10^{16}$ cm. No other observational evidence for the binary black hole model has been reported so far. X-ray observations, having the advantage of looking into the region closed to the black hole, provide a potential tool to find signatures of binary black holes.

In the X-ray band, 4C +73.18 has been observed previously by *Einstein* (Biermann et al. 1981), *EXOSAT* (Biermann et al. 1992, Ghosh & Soundararajaperumal 1992),

Ginga (Lawson & Turner 1997), and by ROSAT in the Survey (Voges et al. 1999) and pointed observations with PSPC (Brunner et al. 1994, and Sambruna 1997) and HRI, respectively. The measured spectra were generally described by a power law. Of particular interest is the detection of a significant iron K_{α} emission line in the Ginga observation, making this object one of the few flat-spectrum radio quasars showing iron K_{α} line. Furthermore, the ROSAT data seem to suggest an absorption column in excess of the Galactic value.

In this paper, we report on results of an X-ray observation of 4C+73.18 in the 0.8–10 keV band performed by the ASCA satellite. The spectral and temporal analysis of the data are presented in § 2 and 3, respectively. A re-analysis of the archival ROSAT PSPC spectrum is also given (§ 2.3). We discuss the implications of the results and summarize the main conclusions in § 4 and § 5, respectively. Errors are quoted at 68% level throughout the paper, unless mentioned otherwise.

2. X-ray spectrum

2.1. ASCA observation and data reduction

4C+73.18 was observed with ASCA (Tanaka et al. 1994) on 12 August, 1997. The Solid-state Imaging Spectrometer (SIS) was operated in 1-CCD faint mode. The data reduction and spectral analysis was performed using FTOOLS (v.4.2) and XSPEC (v.10), respectively. We used the ‘bright 2’ mode data for SIS with the corrections for dark frame error and echo effect applied. After removing hot and flickering pixels, the data screening was performed in the standard way using the following criteria: an elevation angle of 10° , a magnetic cutoff rigidity of $6 \text{ GeV}/c$, and bright Earth angles of 25° for the SIS0 and 20° for the SIS1. The effective exposures for good data interval were 16.8/17.6 ksec for the SIS0/1 and 17.8 ksec for the Gas Imaging Spectrometer (GIS). The source counts were extracted from circular regions of ~ 3.5 and 6 arcmin radius for SIS and GIS, respectively. The background counts were determined in two ways, from blank sky observations at the same region of the detector and from a ‘local’ off-source region of the same observation (at the same off-axis position with the same radius as the source region in the case of GIS). The count rates of the two kinds of background data agree with each other within about 10% relative errors. In the analysis we always used both backgrounds and compared the results but only those obtained by using blank sky data are presented here, for they have a higher signal-to-noise ratio. The averaged net source count rates of the SIS1/2 and GIS3/4 are 0.14 cts/s and 0.13 cts/s, respectively. The spectra of both the two

GIS and SIS detectors were combined¹ and re-binned to have at least 30 counts in each energy bin.

2.2. The ASCA spectrum

2.2.1. A single power law fit

Due to the increasing degradation of the response at low energies the calibration below $\sim 1 \text{ keV}$ is uncertain for the SIS². As a conservative criterion, we ignored the energy band below 0.9 keV ³ (Ikebe, private communication). A simultaneous single power law fit to the combined SIS and GIS spectra is not acceptable (see Table 1) either for free or for fixed Galactic absorption ($N_{\text{H}}^{\text{Gal}} = 7.40 \times 10^{20} \text{ cm}^{-2}$, Dickey & Lockman 1990). Noticeable deviations from a power law can be seen from the residuals in Fig. 1 (a) and (b), which show a spectral hardening above 6 keV and a line-like feature around 1.3 keV. Even ignoring the 1.1–1.5 keV data which covers the line-like feature yielded no acceptable fits. Repeating the same fits (fixing N_{H} at the Galactic value) to the 2–10, 3–10, and 4–10 keV band data gave progressively flattening photon indices $\Gamma = 1.61 \pm 0.06$, $1.48_{-0.10}^{+0.08}$, and $1.37_{-0.18}^{+0.14}$, respectively), indicative of a curved spectral shape in the 0.8–10 keV band (1–13 keV in the quasar frame). This suggests composite spectral models, i.e. a power law plus a soft X-ray component.

The integrated 2–10 keV flux is $6.2 \times 10^{-12} \text{ erg cm}^{-2} \text{ s}^{-1}$, using the mean value of the SIS and GIS measurements, which corresponds to a K-corrected luminosity of $2.9 \times 10^{45} \text{ erg s}^{-1}$ ($q_0 = 0.5$, $H_0 = 50$).

No emission line features were seen at the iron K_{α} line energy. The 90% upper limits on the equivalent width of a 6.4 keV line ranges from 62 to 112 eV (source rest frame) for line-widths ranging from 0.01 to 0.5 keV.

2.2.2. Power law plus soft X-ray component

We have tried the following models for the soft X-ray component: power law (PL), blackbody (BB), disk-blackbody (DBB), and thermal plasma (RS, Raymond-Smith in XSPEC). The results are summarized in Table 1 except for DBB models. The listed temperatures are in the quasar

¹ We found that, for relatively weak sources, the spectrum combining applications in the standard FTOOLS package resulted in unreasonably large statistical errors and thus unrealistically small χ^2 in the spectral fits. We therefore used pure Poissonian errors for the counts in each bin for the combined spectrum. This might slightly overestimate the resulting χ^2 of the fits since systematic uncertainties were not taken into account; however, for relatively weak sources, the uncertainties were dominated by photon statistics.

² ASCA Calibration Uncertainties, 1999, ASCA web page at GSFC, NASA.

³ Fitting an absorbed power law to the 0.6–10 keV SIS spectra gave N_{H} significantly larger than the Galactic value (7.4×10^{20}), 16.0×10^{20} for SIS1 and 9.7×10^{20} for SIS0, which are inconsistent with the GIS spectra.

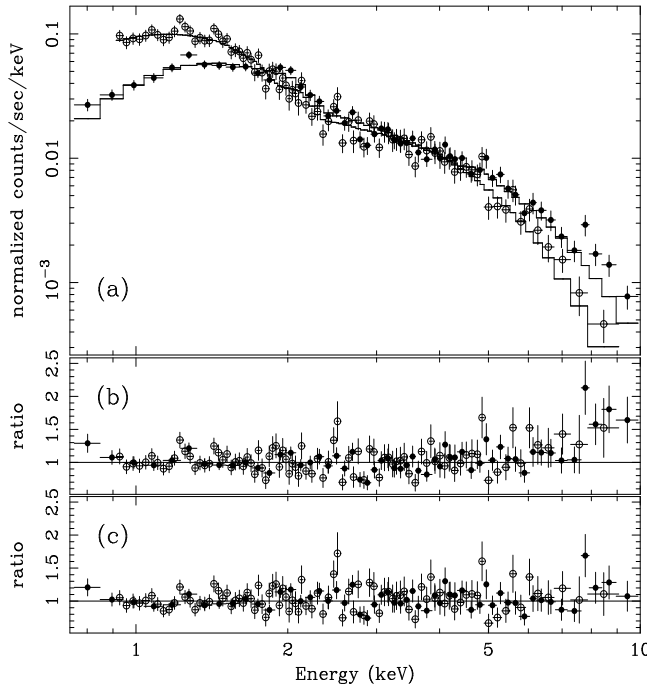


Fig. 1. (a) Simultaneous fit to the SIS (open circles) and GIS (dots) spectra with an absorbed power law (Galactic absorption). (b) The residuals of (a) as the ratio between the data and the fitted model. (c) The residuals of the best fit model composed of a power law with Galactic absorption plus cold reflection, thermal plasma, and an additional Gaussian line (see text).

rest frame. In general, the addition of a soft component improves the fits significantly ($\Delta\chi^2 = 16, 16, 17, 19$ for PL, BB, DBB, RS, respectively); yet the fits remain relatively poor. Ignoring the 1.1–1.5 keV line-like feature improved the fits slightly and made them marginally acceptable, with a significance level $P \sim 0.11$ for PL, 0.13 for BB, 0.16 for DBB, 0.25 for RS, respectively. Thus, the current data are insufficient to impose strong constraints on the spectral form of the soft X-ray component, given the degrading SIS low energy response. On the other hand, as will be discussed below, it is also possible that none of the above models is a good representation of the real spectral shape. The thermal plasma model yields the minimal χ^2 and N_{H} in good agreement with the Galactic value, but, implausibly low metal abundances and a much flatter photon index than the ‘canonical value’ $\Gamma \simeq 1.6$ for flat-spectrum radio quasars.

2.2.3. Reflection component

An additional soft X-ray component seems not to be able to fully account for the spectral hardening. In the case of thermal plasma model, the power law index is too flat ($\Gamma = 1.10^{+0.13}_{-0.53}$), while for the other models the residuals show some remaining excess flux in the highest energy

Table 1. Spectral fits for 4C +73.18

parameters	SIS+GIS	SIS+GIS ^(a)	PSPC
power law			
$N_{\text{H}}^{(b)}$	~ 0	~ 0	$10.9^{+1.2}_{-1.0}$
Γ	$1.69^{+0.04}_{-0.02}$	$1.67^{+0.03}_{-0.02}$	2.25 ± 0.12
$N^{(c)}$	1.67 ± 0.15	1.63 ± 0.16	1.88 ± 0.13
χ^2/dof	1.26/140	1.20/121	0.95/23
power law (fixed $N_{\text{H}} = 7.4 \cdot 10^{20}$)			
Γ	1.79 ± 0.02	1.77 ± 0.02	$1.82^{+0.05}_{-0.06}$
N	1.90 ± 0.07	1.84 ± 0.09	1.63 ± 0.06
χ^2/dof	1.31/141	1.27/122	1.73/24
power law + power law			
N_{H}	26.4 ± 15.5	22.8 ± 21.5	$13.6^{+3.4}_{-2.6}$
Γ	1.14 ± 0.45	1.12 ± 0.60	1.5 (fixed)
Γ_s	3.04 ± 1.04	2.93 ± 1.44	$3.26^{+0.74}_{-0.85}$
χ^2/dof	1.17/137	1.14/118	0.94/22
power law + zbbbody			
N_{H}	~ 0	~ 0	$8.9^{+1.3}_{-0.9}$
Γ	$1.42^{+0.05}_{-0.09}$	1.42 ± 0.08	1.5 (fixed)
kT (keV)	$0.44^{+0.02}_{-0.04}$	$0.44^{+0.04}_{-0.03}$	$0.18^{+0.03}_{-0.02}$
χ^2/dof	1.17/137	1.15/118	0.97/22
power law + zbbbody ($N_{\text{H}} = 7.4 \cdot 10^{20}$)			
Γ	$1.48^{+0.03}_{-0.04}$	$1.49^{+0.04}_{-0.06}$	$1.17^{+0.18}_{-0.30}$
kT	$0.38^{+0.02}_{-0.03}$	$0.37^{+0.03}_{-0.04}$	0.21 ± 0.02
χ^2/dof	1.18/138	1.16/119	0.97/22
power law + thermal plasma			
N_{H}	$8.1^{+4.9}_{-2.7}$	$12.2^{+7.0}_{-4.2}$	$7.3^{+0.6}_{-0.5}$
Γ	$1.02^{+0.22}_{-1.02}$	$1.27^{+0.16}_{-0.15}$	1.5 (fixed)
kT	1.83 ± 0.43	$1.44^{+0.21}_{-0.26}$	$0.84^{+0.18}_{-0.13}$
$A^{(d)}$	0.1 ± 0.1	$0.5^{+1.1}_{-0.3}$	1.0 (fixed)
χ^2/dof	1.16/136	1.08/117	1.07/22
power law + thermal plasma ($N_{\text{H}} = 7.4 \cdot 10^{20}$)			
Γ	$1.10^{+0.13}_{-0.53}$	$1.27^{+0.16}_{-0.26}$	$1.50^{+0.17}_{-0.70}$
kT	$1.76^{+0.73}_{-0.21}$	$1.59^{+0.29}_{-0.21}$	$0.86^{+0.19}_{-0.15}$
A	0.1 ± 0.1	$0.4^{+1.3}_{-0.2}$	0.2 ± 0.2
χ^2/dof	1.15/137	1.08/118	1.08/21
perxav + thermal plasma + Gaussian ($N_{\text{H}} = 7.4 \cdot 10^{20}$)			
Γ	$1.50^{+0.16}_{-0.50}$	$1.41^{+0.22}_{-0.35}$	–
kT	$1.83^{+0.40}_{-0.29}$	$1.62^{+0.30}_{-0.23}$	–
A	0.2 ± 0.2	$0.4^{+0.8}_{-0.3}$	–
$\Omega/2\pi^{(e)}$	$0.58^{+0.47}_{-0.58}$	$0.46^{+0.81}_{-0.46}$	–
$\cos \theta^{(f)}$	$0.97^{+0.03}_{-0.65}$	$0.96^{+0.04}_{-0.90}$	–
$E_{\text{line}}^{(g)}$ SIS	$1.25^{+0.03}_{-0.04}$	–	–
$E_{\text{line}}^{(g)}$ GIS	1.26 ± 0.05	–	–
$I_{\text{line}}^{(h)}$ SIS	$2.1^{+1.1}_{-1.0}$	–	–
$I_{\text{line}}^{(h)}$ GIS	$3.7^{+2.5}_{-2.2}$	–	–
χ^2/dof	1.15/131	1.09/116	–

(a) Excluding 1.1–1.5 keV line-like structure

(b) Column density in units of 10^{20} cm^{-2}

(c) Normalization at 1 keV in units of $10^{-3} \text{ photon cm}^{-2} \text{ s}^{-1} \text{ keV}^{-1}$

(d) Abundances in units of solar value

(e) Solid angle subtended by the reflecting matter

(f) Inclination angle of the normal of the reflecting slab

(g) line energy in units of keV

(h) line intensity in units of $10^{-5} \text{ photon cm}^{-2} \text{ s}^{-1}$

bins. Fitting a broken power law plus thermal plasma model yielded a low energy band index $\Gamma = 1.4$ and a flat index 0.1 in the hard energy range beyond ~ 7 keV. We then tried to include a Compton-reflection component (*pexrav* in XSPEC), in which a Compton thick, neutral (except H and He) slab is irradiated by an X-ray source with a subtended solid angle Ω . The high-energy cutoff was fixed at 500 keV. The fitted photon index became $1.50^{+0.16}_{-0.50}$. However, the improvement of the fit is insignificant and the addition of the reflection component cannot be justified. It should be noted that the model of a power law plus reflection but without a soft component yielded no acceptable fits.

2.2.4. Emission line like feature around 1.3 keV

We now consider the emission line like feature around 1.3 keV. We repeated the same fitting as in § 2.2.3 (RS plus *pexrav* model) by adding a Gaussian line at ~ 1.3 keV with fixed line width $\sigma = 0.01$. The line energies and normalizations were set to be independent for the SIS and the GIS. The best-fit parameters are given in Table 1, and the residuals are shown in Fig. 1 (c). The fit improved with $\Delta\chi^2 = 6.0$. Given four additional parameters involved (the line energies and intensities for both SIS and GIS), the significance for adding the line component is only marginal (at a confidence level slightly less than 90%). The derived equivalent width is 22^{+12}_{-11} eV for the SIS and 31^{+21}_{-20} eV for the GIS data.

It seems unlikely that the excess in Fig. 1 is an instrumental effect as the feature appears in both, the SIS and GIS data at almost identical energies, $1.25^{+0.03}_{-0.04}$ and 1.26 ± 0.05 keV, respectively. The line seems to be narrow, with an apparent width of the order of the detector energy resolution, and to be non-Gaussian, as indicated by the structure of the residuals in Fig. 1 (c). Plotted in Fig. 2 are the confidence contours in the parameter space of the line energy vs. strength, which were obtained by using the GIS data only. We also tried absorption models instead of an emission line to see whether the line-like feature can be accounted for. However, neither an absorption edge nor a notch line fits the data.

2.3. The ROSAT spectrum

To check the consistency of the spectral models derived from ASCA with previous observations, we re-analyzed the archival spectrum of the PSPC pointed observation of 4C+73.18. A power law with neutral absorption model yields a steep photon index ($\Gamma = 2.25 \pm 0.12$) and absorption N_{H} significantly higher than the Galactic value (Table 1). Fixing N_{H} at the Galactic value gives an unacceptable fit ($P = 0.01$) and a flatter index. These results are in agreement with those given in Brunner et al. (1994) and Sambruna (1997). In light of the ASCA spectral modeling, we added a soft X-ray component and performed the same

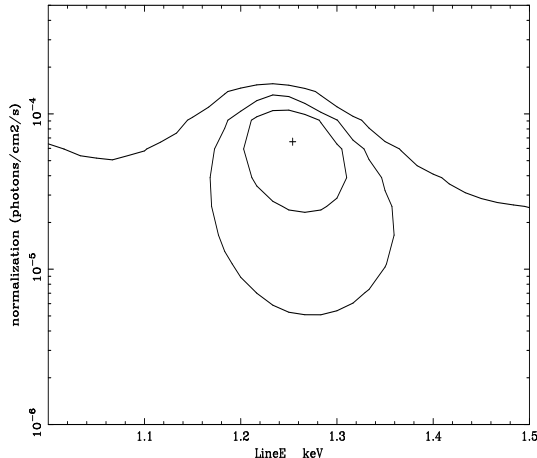


Fig. 2. Confidence contours in the line energy versus strength space for the line fit to the GIS data. The contours are at 68%, 90%, and 99% levels from the center outwards, respectively.

fits as in § 2.2. The results are given in Table 1. Considering the narrow PSPC bandpass, we first fix the photon index of the hard power law at $\Gamma = 1.5$. Adding a blackbody or thermal plasma model both yields the best fits, with $kT = 0.18^{+0.03}_{-0.02}$ and $0.84^{+0.18}_{-0.13}$ keV (source frame), respectively, and an N_{H} consistent with the Galactic value. Fixing N_{H} at the Galactic value and setting Γ as a free parameter gives $\Gamma = 1.50^{+0.17}_{-0.70}$ for the thermal plasma and $\Gamma = 1.17^{+0.18}_{-0.30}$ for the blackbody model, respectively. The fits are insensitive to the metal abundances, and the best fit value is 0.17 ± 0.16 solar. The excess absorption suggested previously is not required, which apparently resulted from fitting a single power law to the steepening part of the curved spectrum toward low energies.

No emission line like feature is seen around 1.25 keV in the ROSAT spectrum. However, the poor energy resolution (40% at 1 keV) makes the PSPC insensitive to such a weak line. The upper limit on the equivalent width of a narrow emission line at 1.25 keV is found to be 74.5 eV at 90% confidence, which is consistent with the ASCA data.

2.4. Summary of spectral fits

The ASCA spectra exhibit a concave curvature which flattens toward high energies. Models composed of a power law and a soft X-ray excess improve the fits significantly, though the spectral shape of the soft component is inconclusive. Such models also fit the previous ROSAT spectrum well, hence the soft X-ray excess in 4C+73.18 seems to be persistent, rather than a transient emission feature. No significant excess X-ray absorption is indicated. No iron K_{α} line is detected. A weak emission line like feature at 1.25 keV is present in both, the SIS and GIS spectra, though the significance is not high. It should be noted that the ASCA spectra are ‘noisy’ above 2 keV, and the spec-

tral fits are relatively poor in general. This may result, at least partly, from source variability as shown below.

3. X-ray variability

3.1. Variability on short time-scales

X-ray light curves were extracted from the source region and binned with a bin size of 96 min (one ASCA orbit) for both the SIS and GIS detectors. The background count rates, estimated from the source free region and normalized to the source region, were subtracted. Plotted in Fig. 3 are the light curves from the SIS detectors only. Small amplitude, but statistically significant flux variations in the 0.5–10 keV band are found (χ^2 test, see Table 2) over the ~ 40 ksec observation. As shown above, the X-rays in the ASCA band are likely composed of a hard power law, a soft component dominating below 1 keV, and a tentative reflection component above 7 keV (9 keV in the source frame). We divided the ASCA energy band into three corresponding bands, i.e. a low (0.5–1 keV), a medium (1–6 keV), and a high (6–10 keV) band. The light curves in Fig. 3 show different temporal variations in the medium band (the power law component) from those in the low and high bands. The medium band flux reveals significantly more variability than the whole band ($\Delta\chi^2 = 4$), whereas the low and high energy band fluxes are consistent with no variations (Table 2). We checked the significance of the relative variations between different bands by testing the constancy of their counts ratios, $C_{1-6\text{keV}}/C_{0.5-1\text{keV}}$ and $C_{1-6\text{keV}}/C_{6-10\text{keV}}$. The probabilities for the χ^2 tests are listed in Table 2. Non-synchronized variations between the medium and low, and the medium and high bands, however, cannot be confirmed. This is likely due to the poor photon statistics in the low and high bands, as well as to the contribution from the underlying power law flux in these two bands. The GIS light curves show very similar variations; however, the large counting errors due to the higher background level makes the GIS insensitive to variability with such small amplitudes.

Table 2. χ^2 test of variability for the SIS fluxes

band (keV)	χ^2 (dof=6)	$P(\chi^2)$	significance
0.5–10	13.5	0.035	yes
0.5–1	5.9	0.43	no
1–6	17.4	0.008	yes
6–10	4.3	0.64	no
Variability of counts ratio			
$C_{1-6\text{keV}}/C_{0.5-1\text{keV}}$	8.1	0.23	no
$C_{1-6\text{keV}}/C_{6-10\text{keV}}$	5.3	0.50	no

Note: we use the critical significance level of $P = 0.05$.

We conclude that the observed short time scale flux variability in 4C+73.18 is mainly attributable to variations of the hard band power law. The variability time

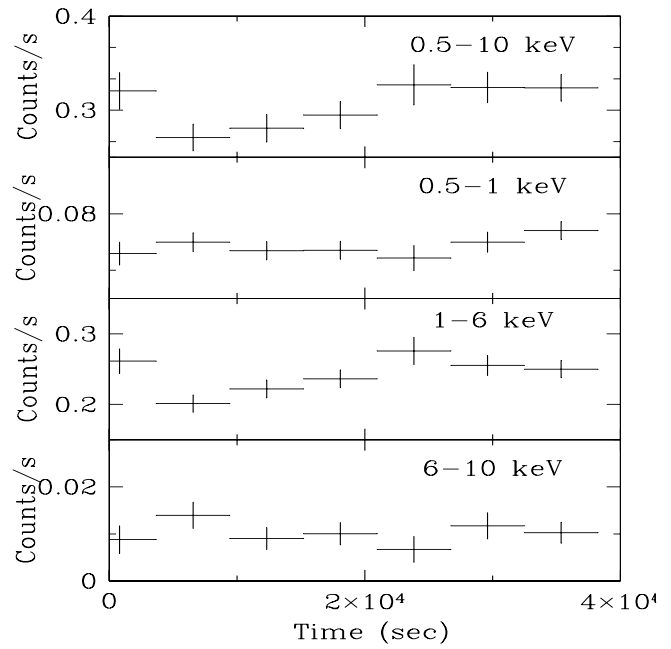


Fig. 3. Background subtracted X-ray light curves of 4C+73.18 from the SIS detectors (SIS0+SIS1) in the whole band (upper panel) as well as in the low, medium, and high passbands. The bin size is 5760 s and the errors are of 1σ .

scale is not obtainable from the relatively short observation interval; however, it could be of the order of the duration of the observation, i.e. 10 hours in the source frame. No statistically significant variations are found for the flux in the 0.1–1 keV band. This result is supported by the lack of variations of the flux in the 0.1–2.4 keV PSPC band on similar time scales during the ROSAT observation ($\chi^2 = 1.06$ for 37 d.o.f., Brunner et al. 1994). The uncorrelated, energy dependent flux variations are consistent with the above models of multi-component X-ray emission.

3.2. Long-term variability

We present in Fig. 4 the long-term X-ray light curve of 4C+73.18, compiled from the flux densities at 1 keV from previous missions. The estimated Ginga flux is an extrapolation of the observed 2–10 keV spectrum and, as discussed below, should be taken as an upper limit due to possible flux contamination from nearby sources. The light curve tends to suggest an overall increase of the 1 keV flux density by a factor of 50% over 18 years of observations.

In addition, prominent flux variations in the hard X-ray band were reported from the EXOSAT observations: the 2–10 keV flux varied by a factor of 2–3 (from $1.5-5.1 \times 10^{-12} \text{ erg cm}^{-2} \text{ s}^{-1}$) on a time scale of about one month (Ghosh & Soundararajaperumal 1992).

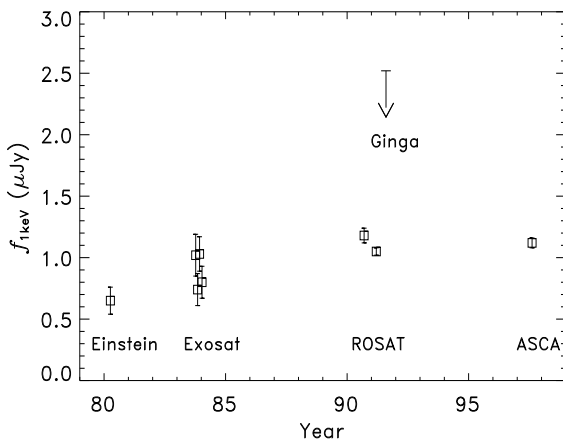


Fig. 4. Historical light curve of the X-ray flux densities of 4C+73.18 measured at 1 keV. The fluxes of *Einstein* and *EXOSAT* observations are taken from Brunner et al. (1994). The two ROSAT data points represent the Survey and pointed observations, respectively. The estimated Ginga flux (taken as an upper limit here; see text) is an extrapolation of the measured 2–10 keV spectrum from Lawson & Turner (1997).

4. Discussion

4.1. Emission from host cluster of galaxies?

As mentioned by Brunner et al. (1994, quoting a private communication) there are indications for a cluster of galaxies around 4C+73.18, which would affect the X-ray spectrum determined from instruments with limited spatial resolution. To investigate the possible role played by an extended X-ray emission component, we fitted a point source plus a β -model (e.g. Gorenstein et al. 1978) of the form

$$S(r) = S_0 \left(1 + \frac{r^2}{r_c^2}\right)^{-3\beta+1/2}$$

to the surface brightness profile of the ROSAT HRI source (with an exposure of 38660 sec). The result is inconclusive; however, a noticeable contribution from a cluster at a flux level greater than a few percent in the HRI energy band can be ruled out.

In the hard X-ray band (0.8–10 keV), no evidence for extended emission is found in the ASCA GIS image. Moreover, no iron K_{α} emission line is detected in the ASCA spectra. It should be noted that the GIS source extraction radius of 6 arcmin corresponds to ~ 1.3 Mpc at the quasar distance, which is about 2–3 times the typical X-ray core radius and hence may well encompass the X-ray emitting region of the host cluster. Taking the typical value of 1 keV for the equivalent width of the iron K_{α} line of cluster emission, the derived $EW < 50$ eV places an upper limit on the flux density of a host cluster of being 7% of the quasar flux at about 5 keV in the observer frame. Thus, we do not find

evidence for noticeable X-ray emission from a host cluster of galaxies.

4.2. The iron line puzzle

One of the interesting results of this work is the non-detection of the iron K_{α} line, which was previously reported from the Ginga observation (Lawson & Turner 1997). The upper limits of the equivalent width is estimated to be 62 eV, in contrast to the measured 185^{+79}_{-74} eV by Ginga. Moreover, the spectrum ($\Gamma = 2.08^{+0.05}_{-0.04}$) is steeper and the flux (8.7×10^{-12} erg cm $^{-2}$ s $^{-1}$) higher for Ginga than for the ASCA observations ($\Gamma = 1.61 \pm 0.06$ and flux 6.2×10^{-12} erg cm $^{-2}$ s $^{-1}$) in the 2–10 keV band. The difference of the two continuum spectra can be seen clearly in Fig. 5. There are two possible explanations to this observed discrepancy, namely, either genuine spectral variations of both the iron line and continuum, or contamination of the Ginga spectrum by other sources. We consider the latter to be more plausible, based on the following arguments.

4.2.1. Iron line variability

It is rare for blazar-type radio quasars to show iron line emission (e.g. Siebert et al. 1996, Lawson & Turner 1997, Reeves et al. 1997, Cappi et al. 1997). X-ray monitoring of 3C 273 also revealed that the iron line was detected in only some but not all of the observations. This effect seems to be dependent on variations of the continuum rather than of the line flux—at a high continuum flux, the line equivalent width decreases or the line is even swamped (e.g. Turner et al. 1990, Cappi et al. 1998). However, this was not the case for 4C+73.18 during the Ginga observation (see below for a discussion on the Ginga flux). If the line did come from the quasar, there must be a variation of the line itself. This may suggest that during the Ginga observation Seyfert like emission from the central AGN was substantially enhanced while the jet emission dimmed since no significant changes were found for the overall flux level.

4.2.2. Iron line from another object?

Given the large field of view (FOV) of $1.1^{\circ} \times 2.0^{\circ}$ (FWHM) and poor energy resolution of Ginga, the association of the detected line with the quasar, and even the presence of the line, may be questionable. We examined X-ray sources in the vicinity of 4C+73.18 which may have fallen into the FOV of the Ginga observation. Within the GIS FOV there is another source detected at a distance of 12 arcmin from the quasar; however, the flux in the Ginga energy band is too low (2.7×10^{-13} erg cm $^{-2}$ s $^{-1}$) to make considerable contribution to the observed Ginga flux.

We next analyzed the data of ROSAT PSPC pointed observation of 4C+73.18, whose 2° FOV covers a large

portion of the Ginga FOV. Among 27 X-ray sources detected (with a detection likelihood larger than 10) in addition to 4C+73.18, we found one source of particular interest. The source is located 43 arcmin away from the quasar and inside the Ginga FWHM field of view (Yamagishi, private communication). It is bright (0.1 counts s⁻¹ in the 0.1–2.4 keV band—40% of the count rate of the quasar) and extended (4 times of the FWHM of the point spread function). This source has been selected from the ROSAT All-Sky Survey as a candidate of, and later confirmed in optical to be, a cluster of galaxies (Boehringer et al. 2000). The ROSAT spectrum, which is of poor photon statistics, can be fitted with thermal bremsstrahlung emission, and the temperature seems to be higher than 3 keV. Though the redshift is unknown, we suggest this X-ray cluster as a likely source of the emission line detected by Ginga.

As a self-consistency check, we compare the line intensity predicted for the cluster with the observed value. The observed line flux by Ginga is $2.55^{+1.08}_{-1.02} \times 10^{-5}$ photon s⁻¹ cm⁻² and the line energy $5.13^{+0.30}_{-0.20}$ keV (observer frame). Assuming a cluster temperature of 6 keV and extrapolating the fitted ROSAT spectrum to higher energies, we expect that Ginga would detect a line flux of $F_{\text{line}} \simeq 4.4f \text{EW}/(1+z) \times 10^{-5}$ photon s⁻¹ cm⁻², where EW is the line equivalent width (in units of keV, in the source frame) and f the Ginga off-center detection efficiency at the source position ($f \simeq 0.6$ in this case). For a redshift close to that of the quasar, $z \sim 0.3$, we have $F_{\text{line}} \sim 2.0 \text{EW}$ (10⁻⁵ photon s⁻¹ cm⁻²), which is compatible with the observed value for a range of line equivalent width from several hundred eV to 1 keV. In this case, the measured Ginga line energy implies that the cluster is at a redshift range $0.23 \leq z \leq 0.36$ for a 6.7 keV K_{α} line. However, no firm conclusion can be drawn on the origin of the line until the redshift of the cluster is available.

4.2.3. The Ginga continuum flux

The estimated continuum flux from the cluster, using the above parameters, is $\sim 2 \times 10^{-12}$ erg cm⁻² s⁻¹ in 2–10 keV, which may account for the measured flux excess for Ginga over the ASCA measurement. Further, though the rest of the sources in the PSPC FOV are too faint and soft to be considerable contributors to the observed Ginga flux, they may account for the steepening of the Ginga spectrum in the soft X-rays. The total PSPC count rate of sources in the vicinity of 4C+73.18 turned out to be ~ 0.36 counts s⁻¹, 1.3 times higher than that of quasar itself. Thus we suggest that the excess fluxes of the Ginga observation over those of ROSAT and ASCA in the soft and medium X-ray band (see Fig. 5) could be, at least partly, accounted for by emission from the cluster of galaxies and other nearby soft X-ray sources. The genuine X-ray flux of the quasar might be comparable with that of ASCA and ROSAT, though quantitative estimates can only be obtained by detailed modeling.

4.3. The soft X-ray excess

The presence of an excess flux at energies below ~ 1 keV over the extrapolation of the hard band spectrum is evident from the curved spectrum in the ASCA band and the uncorrelated variations in the soft (0.5–1 keV) and hard (1–6 keV) band. The latter was also reported from the *EXOSAT* observations (Ghosh & Soundararajaperumal 1992). However, the spectral shape of the soft excess is uncertain. We show in Fig. 5 the optical to X-ray energy distribution of 4C+73.18, which is very similar to that of 3C 273. The optical-UV spectral shape, though with sparse data points, is suggestive of a prominent UV component which peaks at shortward 1300 Å or above 10^{15.3} Hz (the ‘blue bump’), and probably extends into the EUV band. It is natural to regard the soft X-ray excess to be the high-energy tail of the UV bump, which results from Compton up-scattering disk photons to higher energies by hot gas.

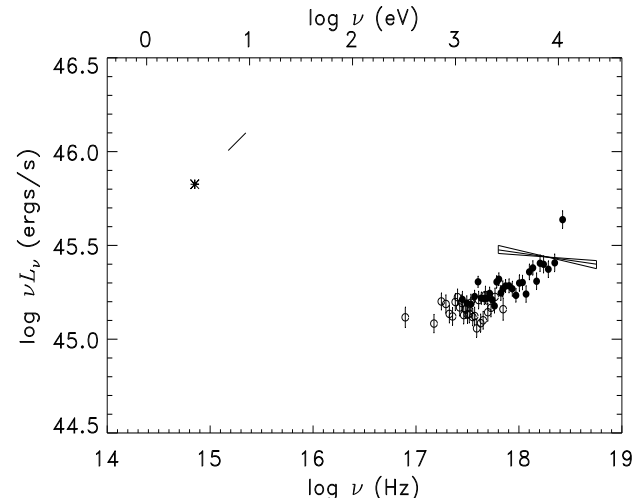


Fig. 5. The optical to X-ray spectral energy distribution of 4C+73.18 in the source rest frame ($q_0 = 0, H_0 = 50$). The UV (*HST*) spectrum is taken from Laor et al. (1995). The open circles are the ROSAT data and the filled dots the ASCA GIS data. For a comparison, the power law spectrum obtained in the Ginga observation is over-plotted.

When fitted with a thermal emission model, the temperature kT_{ex} (e.g. 0.4 keV for blackbody) is somewhat higher than those obtained in a few core-dominated radio quasars for which kT_{ex} was relatively well determined, e.g. ~ 0.1 keV in 3C 273 (e.g. Turner et al. 1990, Bühler et al. 1994, Cappi et al. 1998). The higher kT_{ex} could imply that the up-shift of the energy of disk photons is more pronounced in 4C+73.18 than in 3C 273. The hot gas may be the skin-type coronae surrounding the accretion disks, as discussed in detail in, e.g., Czerny & Elvis (1987). In the Czerny & Elvis model, the high kT_{ex} im-

plies that the quasar is likely radiating at a luminosity around the Eddington luminosity (see Fig. 7 of Czerny & Elvis 1987). If this is true, a UV luminosity of the order $\sim 10^{46}$ erg s $^{-1}$ (see Fig. 5) implies a central mass of the order of $8 \times 10^7 M_{\odot}$ in 4C+73.18. This value is close to the mass of the binary black hole system ($10^8 M_{\odot}$) estimated by Roos et al. (1993) by modeling the wiggles of the VLBI jet. Other sources of the hot gas might be the base of the relativistic jet where it emerges from the accretion disk, as proposed by Mannheim et al. (1995). These scenarios all require a small inclination angle of the disk (or the jet, respectively) to the observer, in agreement with the super-luminal motion observed in this source. Finally, the result is consistent with the findings by Brinkmann et al. (1997) that the soft X-ray excess tends to be more significant in core-dominated than in lobe-dominated quasars.

In the soft X-ray band, the spectral analyses in § 2 indicate a higher temperature for the soft thermal component in the ASCA than in the ROSAT observations. This may well be a genuine spectral change, as the observations are about 6 years apart. The conclusion, however, must be drawn with caution due to the inter-instrument calibration uncertainties. There have been reports that the ROSAT PSPC tends to give steeper spectra than ASCA, even within the overlapping bandpass (e.g. Iwasawa et al. 1999). Such an effect might play a role in comparing the temperatures derived from the two instruments.

4.4. The hard X-ray continuum: emission from jet

The observed flat power law continuum in the hard X-ray band is typical for flat-spectrum radio-loud quasars. The inferred time scale of variations of the power law continuum might be as short as of the order of hours. These factors, as well as the lack of an iron K_{α} line, are typical signatures of the radio-jet-linked X-ray emission in radio-loud AGN, which is strongly beamed by relativistic bulk motion. Thus the ASCA observation provides strong evidence for the idea that the hard X-rays in 4C+73.18 are emitted predominantly from the jet (via inverse Compton scattering). Such mechanism has been tested in detail in a few similar super-luminal quasars (e.g. 3C 345, Unwin et al. 1994).

To investigate the contribution of possible Seyfert-like emission, we tried to include a steep power law (fixing $\Gamma = 1.9$) as well as reflection in the above fittings. No acceptable fits were obtained when a significant Seyfert-like emission component was included. Though, as shown in § 2.2, including a reflection model can account for the tentative excess fluxes in the highest energy bins of the ASCA spectra, the addition of this component is not justified statistically by the data. Given the lack of an iron line and that the continuum is dominated by beamed jet emission, a significant reflection component can not be physically justified either.

4.5. The 1.3 keV emission line feature

A marginal, narrow line feature at 1.25 keV is suggested to be present in 4C+73.18. It is not clear from the current data whether this is a real line or an instrumental artifact, though the latter seems unlikely given that this feature appears in both the co-added SIS and GIS data at almost identical energies. If interpreted as associated with the quasar, the line energy corresponds to 1.63 ± 0.05 and 1.64 ± 0.07 keV in the quasar frame for the SIS and GIS, respectively. No known emission lines have been found or are expected to be present around these energies. The closest line is the He-like MgXI transition at 1.58 keV.

Interestingly enough, using ASCA data Yaqoob et al. (1998) reported the discovery of a peculiar narrow emission line ($EW = 59^{+38}_{-34}$ eV), which has never been seen in any other AGN, in another flat-spectrum quasar PKS 0637-752 (redshift 0.654). The line energy in quasar frame is at 1.60 ± 0.07 , which is strikingly close to what we found in this work. Therefore, the line-like feature in 4C+73.18 provided the first independent evidence for the presence of such an emission line, though the statistical significance of the presence of the line is low. It seems unlikely that the match of the line energies in two quasars with different redshifts is a coincidence. The identification of this line is, however, unknown (see Yaqoob et al. 1998 for a discussion of the possibilities). If the emission line feature found in this work is real and identical to that of Yaqoob et al. (1998), the obtained $E_{\text{line}} \sim 1.6$ keV should be the line energy in the rest frame, rather than a Doppler-shifted value due to the in- or out-flow of the emitting gas. Otherwise it is hard to explain why the bulk motions are exactly the same in the two quasars.

5. Conclusions

The flat-spectrum, super-luminal quasar 4C+73.18 resembles the well studied, similar object 3C 273 in some basic properties in the soft-to-medium X-ray band. Rapid, small amplitude ($\sim 25\%$) flux variations were detected in the 1–10 keV band on a tentative time scale of the order of 10 hours, whereas no significant variations were found for the soft X-rays below 1 keV. The 0.8–10 keV spectrum exhibits a curvature, which can be modeled by a power law plus a soft component. Both, the X-ray spectrum and the uncorrelated flux variations provide strong evidence for the presence of a soft X-ray excess over the extrapolation of the hard band power law, which might be the high-energy extension of the UV bump emission. The underlying continuum is flat, with a power law photon index of 1.1–1.5, depending on the spectral model adopted for the soft component. The dominance of the flat power law over possible Seyfert-like emission, together with the short time scale variability, are naturally explained by beaming models for the jet, which is estimated to be observed at an inclination angle about 10 degree. No iron K_{α} emission line

is detected, in contrast to the significant line reported in a previous Ginga observation, which is most likely contamination from another source. A weak emission line-like feature around 1.25 keV (1.6 keV in the quasar frame) seems to be present in both the SIS and GIS spectra, though the significance is not high. The line energy is identical to that of a mysterious emission line in the flat-spectrum quasar PKS 0637-752 reported by Yaqoob et al. (1998).

Acknowledgements. WY thank Y. Ikebe for the help regarding the ASCA data analysis and discussion on the X-ray cluster in the Ginga FOV, and also thank S. Xue for useful discussions. The authors thank I. Yamagishi at ISAS for getting the attitude information of the Ginga observation. We thank the Northern ROSAT All-Sky (NORAS) team for providing the identification results on the cluster of galaxies before publication. WY is grateful to Prof. J. Trümper and Dr. W. Voges for the financial support during the visit at MPE, and also to Beijing Astronomical Observatory for the financial support and to Prof. J. Chen at Beijing Astrophysics Center for hospitality, where part of the research was done. WY acknowledges support at NASDA by a STA fellowship. MG acknowledges partial support from the European Commission under contract number ERBFMRX-CT98-0195 (TMR network “Accretion onto black holes, compact stars and protostars”).

References

Biermann P.L., Duerbeck H., Eckart A., et al., 1981, *ApJL* 247, 53

Biermann P.L., Schaaf R., Pietsch W., et al., 1992, *A&AS* 96, 339

Boehringer H., et al. 2000, *ApJ* submitted

Brinkmann W., Yuan W., Siebert J., 1997, *A&A* 319, 413

Brunner H., Lamer G., Staubert R., Worrall D.M., 1994, *A&A* 287, 436

Bühler P., Courvoisier T.J.-L., Staubert R., 1994, *A&A* 287, 433

Cappi M., Matsuoka M., Comastri A., et al., 1997, *ApJ* 478, 492

Cappi M., Matsuoka M., Otani C., Leighly K.M., 1998, *PASJ* 50, 213

Czerny B., Elvis M., 1987, *ApJ* 321, 305

Dickey J.M., & Lockman F.J. 1990, *ARA&A* 28, 215

Eckart A., Witzel A., Biermann P., et al., 1985, *ApJL* 296, L23

Fichtel C.E., Bertsch T.L., Chiang J., 1994, *ApJS* 94, 551

Ghisellini G., Padovani P., Celotti A., Maraschi L., 1993, *ApJ* 407, 65

Ghosh K.K., Soundararajaperumal S., 1992, *MNRAS* 254, 563

Gorenstein P.D., Fabrikant D., Topka K., Harnden F.R., Tucker W.H., 1978, *ApJ* 224, 718

Hummel C.A., Schalinski C.J., Krichbaum T.P., et al., 1992, *A&A* 257, 489

Iwasawa K., Fabian A.C., Nandra K., 1999, *MNRAS* 307, 611

Jiang D.R., Cao X.W., Hong X., 1998, *ApJ* 494, 139

Johnston K.J., Simon R.S., Eckart A., et al., 1987, *ApJL* 313, 85

Kühr H., Pauliny-Toth I.I.K., Witzel A., Schmidt J., 1981, *AJ* 86, 854

Laor A., Bahcall J.N., Jannuzzi B.T., Schneider D.P., Green R.F., 1995, *ApJS* 99, 1

Lawson A.J., Turner M.J.L., 1997, *MNRAS* 288, 920

Mannheim K., Schulte M., Rachen J., 1995, *A&A* 303, L41

Murphy D.W., Browne I.W.A., Perley R.A., 1993, *MNRAS* 264, 298

Murphy D.W., Tingay S.J., Preston R.A., et al., 1999, Elsevier preprint

Reeves J.N., Turner M.J.L., Ohashi T., Kii T., 1997, *MNRAS* 292, 468

Roos N., Kaastra J.S., Hummel C.A., 1993, *ApJ* 409, 130

Sambruna R., 1997, *ApJ* 487, 536

Siebert J., Matsuoka M., Brinkmann W., Cappi M., et al., 1996, *A&A* 307, 8

Tanaka Y., Inoue H., Holt S.S., 1994, *PASJ* 46, L37

Turner M.J.L., Williams O.R., Courvoisier T.J.-L., 1990, *MNRAS* 244, 310

Unwin S.C., Wehrle A.E., Urry C.M., et al., 1994, *ApJ* 432, 103

Voges W., Aschenbach B., Boller Th., et al., 1999, *A&A* 349, 389

Witzel A., Schalinski C.J., Johnston K.J., et al., 1988, *A&A* 206, 245

Yaqoob T., George I.M., Turner T.J., et al., 1998, *ApJL* 505, 87